EDGE ARTICLE

Check for updates

All publication charges for this article have been paid for by the Royal Society of Chemistry

Two-photon brightness of NIR-emitting, atomically precise DNA-stabilized silver nanoclusters†

Agata Hajda, [a] Rweetuparna Guha, [b] Stacy Marla Copp [bcde] and Joanna Olesiak-Bańska *[a]

Near-infrared (NIR) emitters with high two-photon absorption (2PA) cross-sections are of interest to enable *in vivo* imaging in the tissue transparency windows. This study explores the potential of DNA-stabilized silver nanoclusters (Ag$_N$-DNAs) as water-soluble two-photon absorbers. We investigate 2PA of four different atomically precise Ag$_N$-DNA species with far-red to NIR emission and varying nanocluster and ligand compositions. 2PA cross-sections, σ_2, were determined by two-photon excited luminescence (2PEL) technique for a wide wavelength range from 810 to 1400 nm. The Ag$_N$-DNAs exhibited reversed strength of corresponding transitions in the two-photon regime, as compared to one-photon, which further demonstrates the complex photophysics of these emitters. Maximal 2PA cross-section value (~582 GM) was observed for (DNA)$_3$[Ag$_{21}$]$^{15+}$, which is stabilized by 3 DNA oligomers. (DNA)$_2$[Ag$_{16}$Cl$_2$]$^{8+}$ presented distinct 2PA behavior from the Ag$_N$-DNAs without chlorido ligands, with a high 2PA of 176 GM at 1050 nm. Our findings support the potential of Ag$_N$-DNAs as NIR-to-NIR two-photon probes that are both excited and emit in the NIR. Their high σ_2 and fluorescence quantum yield values result in superior two-photon brightness on the order of ~10^2 GM, significantly higher than water-soluble organic fluorophores.

Introduction

DNA-stabilized silver nanoclusters (Ag$_N$-DNAs) are an emerging class of biocompatible fluorescent nanomaterials with sequence-tuned optical properties.[1–3] These ultrasmall emitters have unique and diverse photoluminescence properties that span visible and near-infrared (NIR) wavelengths. The optical properties of Ag$_N$-DNAs depend strongly on the size, shape, and effective valence electron count of the nanocluster core, which are governed by the nucleobase sequence of the DNA oligomer template.[4–6] Thus, DNA oligomer selection enables tunable design of Ag$_N$-DNA properties,[7,8] making Ag$_N$-DNAs promising and versatile emitters to meet the needs of bioimaging.

Recent tandem efforts to harness machine learning-guided experiments and to prepare and investigate atomically precise Ag$_N$-DNA species have accelerated the discovery of Ag$_N$-DNAs.[9–11] Many recently discovered Ag$_N$-DNAs emit at NIR-I and NIR-II

wavelengths (700–1000 nm and 1000–1300 nm, respectively)[12–15] with high fluorescence quantum yields[16] (FQY, ϕ) compared to other NIR emitters, such as organic dyes. Water soluble NIR emitting probes are highly desirable for optical imaging of biological samples because scattering, absorption, and autofluorescence of tissues are significantly reduced at NIR wavelengths compared to visible wavelengths.[17,18] The remarkably high FQY and inherent water solubility of NIR Ag$_N$-DNAs make these promising emitters for overcoming the issue of low FQY of NIR-emitting organic fluorophores, which limit *in vivo* fluorescence imaging.

In contrast to their one-photon (1P) properties, the nonlinear optical (NLO) properties of Ag$_N$-DNAs have been far less explored. Two-photon absorption (2PA) is a third order NLO phenomenon that occurs upon simultaneous absorption of two photons, each with half the excitation energy of the chromophore, thereby exciting an electron from the ground state to the excited state. This excitation process requires high-intensity pulsed laser irradiation and is induced at long wavelengths, which are more favorable for deeper penetration into biological samples. 2PA can be followed by two-photon excited fluorescence (2PEF), which enables two-photon fluorescence microscopy (2PFM). 2PFM at NIR-I or NIR-II wavelengths[19] presents multiple advantages compared to the standard 1P fluorescence microscopy, such as deeper sample penetration, reduced phototoxicity and photobleaching, 3D imaging within tissues, selective excitation of femtoliter-scale volumes, and visualization over long time periods (longitudinal imaging).[20–25]

[a]Institute of Advanced Materials, Wroclaw University of Science and Technology, Wrocław, Poland. E-mail: joanna.olesiak-banska@pwr.edu.pl

[b]Department of Materials Science and Engineering, University of California, Irvine, CA 92697, USA

[c]Department of Chemistry, University of California, Irvine, CA 92697, USA

[d]Department of Physics and Astronomy, University of California, Irvine, CA 92697, USA

[e]Department of Chemical and Biomolecular Engineering, University of California, Irvine, CA 92697, USA

† Electronic supplementary information (ESI) available. See DOI: https://doi.org/10.1039/d4sc05853d

Atomically precise silver or gold nanoclusters (Ag/Au NCs) were reported as strong two-photon absorbers.[26–30] 2PA cross-section (σ_2, expressed in Goeppert-Mayer units, GM) for Ag/Au NCs varies from ~10^2 GM to ~10^5 GM and is dictated by nanocluster properties, such as the number of metal atoms, protecting ligands, and doping with other metal atoms.[26–28] However, Ag/Au NCs generally display low ϕ and low two-photon brightness (defined as $\sigma_{2,b} = \phi \times \sigma_2$), limiting their relevance in 2PFM. Early studies of 2PA of Ag$_N$-DNAs suggested the promise of these emitters for 2PFM, but these studies preceded the robust development of purification strategies to produce Ag$_N$-DNA emitters with defined chemical compositions.[31,32] While the 2PA of atomically precise Ag$_N$-DNAs has not been explored in detail, application of this effect is now emerging.[33]

To advance *in vivo* fluorescence imaging, it is a major goal to develop water-soluble, 2PEF probes that both excite and emit at NIR wavelengths with high FQY and high two-photon brightness ($\sigma_{2,b}$ above 50 GM).[34,35] In this study, we investigate 2PA of four different atomically precise Ag$_N$-DNAs with far-red to NIR emission, which were recently investigated by Guha, *et al.*[5] We find that 2PA spectra of the four Ag$_N$-DNAs, measured from 810 nm to 1400 nm, show significant differences between 1P and two-photon (2P) response. We then present a detailed analysis of NLO properties (specifically two-photon absorption) of the NIR-emissive Ag$_N$-DNA with chlorido ligands and known X-ray crystal structure, (DNA)$_2$[Ag$_{16}$Cl$_2$]$^{8+}$. Finally, we compare the 2P brightness of Ag$_N$-DNAs to organic fluorophores and commercially used NIR markers, demonstrating their utility for applications in NIR-to-NIR 2P bioimaging.

Results and discussion

To investigate the NLO properties of far red and NIR emitting Ag$_N$-DNAs, we selected four Ag$_N$-DNAs with different molecular compositions, including total number of Ag atoms, effective valence electron count (N_0), and the numbers of DNA oligomer ligands (n_s) and chlorido ligands (Table 1). Emitters were selected from a recent study by Guha, *et al.*, which reported the molecular compositions and one-photon absorbance (1PA) and emission spectra of four distinct structural/compositional groups of HPLC-purified far-red to NIR emitting Ag$_N$-DNAs.[5] One emitter from each group was selected to study the breadth of possible 2PE properties of far red and NIR emitting Ag$_N$-DNAs. To ensure agreement with past studies,[5] molecular compositions were confirmed by negative-ion mode

electrospray ionization mass spectrometry (see Experimental methods and ESI†), and 1P optical properties of the Ag$_N$-DNAs (absorption and emission) were measured to ensure consistency with prior reports. For the first time, we present one-photon excitation (1PE) spectra of these clusters (Fig. 1). 1PA and 1PEL maxima, FQY, and Stokes shifts are reported in Table 1, and Fig. 1 presents 1P properties of the four Ag$_N$-DNAs.

Fig. 1 shows that the most prominent Ag$_N$-DNA excitation peaks are Gaussian-shaped bands located at the longest wavelength transition in 1PA, indicating that these emitters follow Kasha's rule. We observe no difference in shape or intensity of peaks in 1PA and one-photon excitation (1PE) spectra for **Ag$_{21}$-DNA** (Fig. 1b) and **Ag$_{16}$-DNA-Cl$_2$** (Fig. 1c). For **Ag$_{15}$-DNA**, the peak bands in 1PA and 1PE occur at the same wavelength, but the ratio of the longest-wavelength band and the band located between 400 and 450 nm is significantly higher in 1PE than in 1PA (Fig. 1a). The most significant deviations between 1PA and 1PE are observed for **Ag$_{19}$-DNA** (Fig. 1d). This emitter's 1PE spectrum contains four distinct peaks (347 nm, 401 nm, 450 nm, and 620 nm), while far more peaks are observed in the 1PA spectrum, as previously reported.[5] This suggests that absorption at certain wavelengths does not result in radiative recombination and fluorescence emission for **Ag$_{19}$-DNA**. **Ag$_{15}$-DNA**, **Ag$_{21}$-DNA**, **Ag$_{19}$-DNA** exhibit Stokes shifts between 0.2 and 0.3 eV whereas, **Ag$_{16}$-DNA-Cl$_2$** displays a Stokes shift of 0.7 eV (Table 1).[15] Comparison with FQY shows that energy gap law does not hold for these nanoclusters. **Ag$_{21}$-DNA** displays a high 73% FQY at room temperature in aqueous solution,[16] which is unprecedented for NIR emitters, however it displays the lowest Stokes shift.

Ag$_{16}$-DNA-Cl$_2$ has molecular composition (DNA)$_2$[Ag$_{16}$Cl$_2$]$^{8+}$; *i.e.* the species is stabilized by two copies of the ssDNA template and two additional chlorido ligands, which significantly contribute to nanocluster stability and optical properties.[9] **Ag$_{16}$-DNA-Cl$_2$** is the only Ag$_N$-DNA in this study with a reported high-resolution X-ray crystal structure (and one of only two Ag$_N$-DNA species with high-resolution structural information about both nanocluster core and ligand shell reported to date).[36] This emitter has 26% FQY and a high Stokes shift of 0.7 eV, implicating a large energy difference between the Franck–Condon excited state and the S$_1$–S$_0$ transition (fluorescence). The emitter has been well-studied by the Vosch group.[15,37–40] Theoretical analysis of its 1PA properties identified silver → silver, silver → base and base → silver electronic transitions.[41]

Table 1 Composition and optical properties of Ag$_N$-DNAs, selected from a previous study.[5] n_s: number of ssDNA template stabilizing the Ag$_N$-DNA, N_0: effective valence electrons of Ag$_N$-DNAs, 1PA: one-photon absorption, FQY: fluorescence quantum yield, 1PEL: one-photon excited luminescence

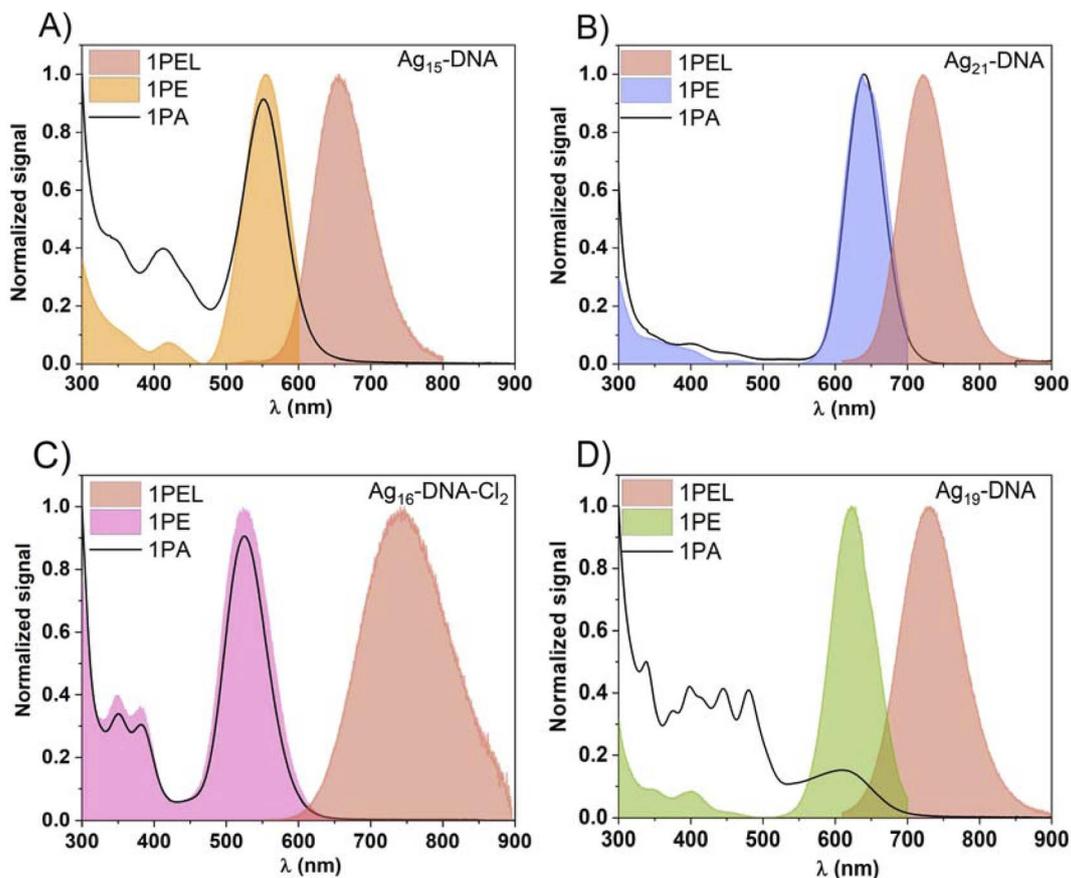| Name	Molecular formula	DNA sequence (5′ to 3′)	n_s and no. of Cl$^-$ ligands	N_0	1PA (nm)	1PEL (nm)	FQY, ϕ [%]	Stokes shift (eV)
Ag$_{15}$-DNA	(DNA)$_2$[Ag$_{15}$]$^{9+}$	ACCAATGACC	2 and 0	6	550	652	11	0.35
Ag$_{21}$-DNA	(DNA)$_3$[Ag$_{21}$]$^{15+}$	CCCGGAGAAG	3 and 0	6	640	721	73 (ref. 16)	0.22
Ag$_{16}$-DNA-Cl$_2$	(DNA)$_2$[Ag$_{16}$Cl$_2$]$^{8+}$	CACCTAGCGA	2 and 2	6	525	744	26 (ref. 15)	0.70
Ag$_{19}$-DNA	(DNA)$_2$[Ag$_{19}$]$^{11+}$	GCGCAAGATG	2 and 0	8	480, 615	730	16	0.31

Fig. 1 Comparison between 1PE (one-photon excitation), 1PA (one-photon absorption, black curve), and 1PEL (one-photon excited luminescence) spectra of (A) Ag_{15}-DNA, (B) Ag_{21}-DNA, (C) Ag_{16}-DNA-Cl_2, and (D) Ag_{19}-DNA.

Finally, **Ag_{19}-DNA** has molecular composition $(DNA)_2[Ag_{19}]^{11+}$ and contains 8 effective valence electrons ($N_0 = 8$), unlike the $N_0 = 6$ of the rest of the Ag_N-DNAs studied here. Because $N_0 = 8$ is a magic number for spherical superatoms,[42] and due to its distinctly different absorption and circular dichroism spectra, **Ag_{19}-DNA** has been hypothesized to possess spheroidal nanocluster geometry[43] rather than the rod-shaped structures of $N_0 = 6$ Ag_N-DNAs.[44]

After characterization of one-photon properties, we measured the NLO properties of the Ag_N-DNA species. The 2PA cross-sections, σ_2, of Ag_N-DNAs and reference samples (Styryl 9M or LDS-698) were evaluated by two-photon excited luminescence (2PEL) technique using femtosecond pulsed laser excitation in a wide range of wavelengths (see Experimental section).[45] As a luminescence-based technique, 2PEL provides information about 2PA cross-section values only for wavelengths at which 2PE leads to luminescence.[26] In systems for which absorption perfectly overlaps with excitation, 2PA spectrum determined with 2PEL can be directly compared with 1PA. However, in systems for which absorption differs from excitation, the measured 2PA spectrum should be compared with the 1PE spectrum. Because excitation and absorption spectra differ for **Ag_{15}-DNA** and **Ag_{19}-DNA** (Fig. 1), we compare 2PA cross-sections to 1PE spectrum. Wavelength ranges were selected such that emission wavelengths do not interfere with the

excitation wavelength range. Moreover, the 2P nature of the observed processes was determined based on the quadratic dependence of photoluminescence intensity (PL intensity) on the incident laser power, P, which indicates a two-photon process in Ag_N-DNAs (the slope of $\log$(PL intensity) $vs.$ $\log(P)$ plots equal $\sim$2.0, Fig. S7†).[46] The values of $\sim$1.9 support a 2P process (small deviations from 2.0 were also seen for reference organic dyes with known 2P behaviour). In case of lower values, contributions from upconversion may be present, as is observed for **Ag_{21}-DNA** for excitation <850 nm (Fig. S7b†). Therefore, it should be noted that σ_2 values for **Ag_{21}DNA** at 810 and 820 nm may have contributions from 1P processes. **Ag_{19}DNA** seems to have significant one-photon process contribution at wavelengths below 980 nm (Fig. S7†), nevertheless transitions involving higher energy states are the most prominent under fs laser excitation. Due to this fact, we present results for **Ag_{19}DNA** in the ESI,† and the measured 2PA spectra for **Ag_{19}DNA** presented in Fig. S8† need to be considered as qualitative. Taking into account, that there is no other experimental or theoretical data for this nanocluster, its response under fs laser illumination needs extended studies, out of the scope of this manuscript. **Ag_{19}-DNA** will be excluded from further comparisons with the other nanoclusters. We ensure lack of photobleaching by using low laser power $\sim$10 mW and a short 5 s exposure time,

with samples exposed to laser irradiation only during signal collection.

Fig. 2 compares the σ_2 values of Ag_N-DNAs to their 1PE spectra. Ag_N-DNAs exhibit maximum σ_2 values of several hundred GM at <950 nm, which corresponds to one-photon transitions at <475 nm. At longer wavelengths, two different types of σ_2 behavior are observed. **Ag$_{15}$-DNA** and **Ag$_{21}$-DNA** exhibit significantly lower σ_2 above *ca.* 1000 nm, in the range of the most prominent $S_1 \rightarrow S_0$ transitions in the 1P regime. In contrast, the 2PA spectrum of **Ag$_{16}$-DNA-Cl$_2$** is distinctly different, with similar σ_2 values at 800 nm and 1050 nm (Fig. 2c).

1PE and 2PA spectra can be compared using the ratio of intensity of higher energy to lower energy transitions in 1PE and 2PA spectra. For **Ag$_{15}$-DNA**, the ratio between 1PE transitions at 420/550 nm is ∼1 : 20. In contrast, the 2PA ratio at 840/1100 nm is 17 : 1. Thus, this emitter displays a reversal of the intensities of 2P transitions compared to 1P transitions.

For **Ag$_{21}$-DNA**, σ_2 is largest for 820 nm and 940 nm excitation, which overlap with low-intensity peaks in the 1PE spectrum (Fig. 2b). The 2PA is nearly zero between 1000 and 1150 nm, similar to 1PE in the 500–550 nm range. However, as mentioned before, the dominant 1PE peak at 640 nm is not the most prominent in 2PA (Fig. 2b). A closer look at 1PE between 400–500 nm (Fig. S2†) shows that high σ_2 bands correlate with very weak 1P $S_0 \rightarrow S_n$ transitions (where $n > 1$). The ratio of 1P transition intensity at 410/460/635 nm is ∼3 : 1 : 67, while for 2PA (at double wavelength) the ratio is 50 : 35 : 1.

For **Ag$_{16}$-DNA-Cl$_2$**, the locations of 2PA transitions are well-aligned with 1PE transitions (Fig. 2c). Surprisingly, however, the 2PA band at longer wavelengths has one order of magnitude higher σ_2 value than the other three Ag_N-DNA species. This **Ag$_{16}$-DNA-Cl$_2$** is discussed in more detail later.

A trend of opposite strength of 1PE and 2PA bands is observed in **Ag$_{15}$-DNA**, **Ag$_{21}$-DNA** and **Ag$_{16}$-DNA-Cl$_2$**. Past studies of unpurified Ag_N-DNAs by Patel, *et al.*[32] reported a similar phenomenon where two-photon excitation (2PE) was more prominent at shorter wavelengths. Thus, such opposite strength of 1PA and 2PE bands could be a more general observation for this type of nanostructures could be a more general observation for this type of nanostructures. 1P and 2P transitions may follow distinct selection rules and resonant enhancements of selected transitions in 2PA, thus giving rise to the possibility of such phenomena. Generally, in molecules with more complex energy landscapes like porphyrins[47] or fluorescent proteins,[48] resonance effects with various electronic or vibrational states contribute to the enhancement of certain 2P transitions. In fluorescent proteins, 2PA corresponding to $S_0 \rightarrow S_1$ transition is often less prominent than for transitions at shorter wavelengths, which gain intensity due to the resonant enhancement effect related to the proximity of virtual state energy (at 1/2 transition energy) and real S_n state.[49] Such a phenomenon may exist in Ag_N-DNAs.

Ag$_{16}$-DNA-Cl$_2$ has one order of magnitude higher σ_2 at longer wavelengths than the other Ag_N-DNAs. **Ag$_{16}$-DNA-Cl$_2$** is distinct for containing chlorido ligands. As one of the most
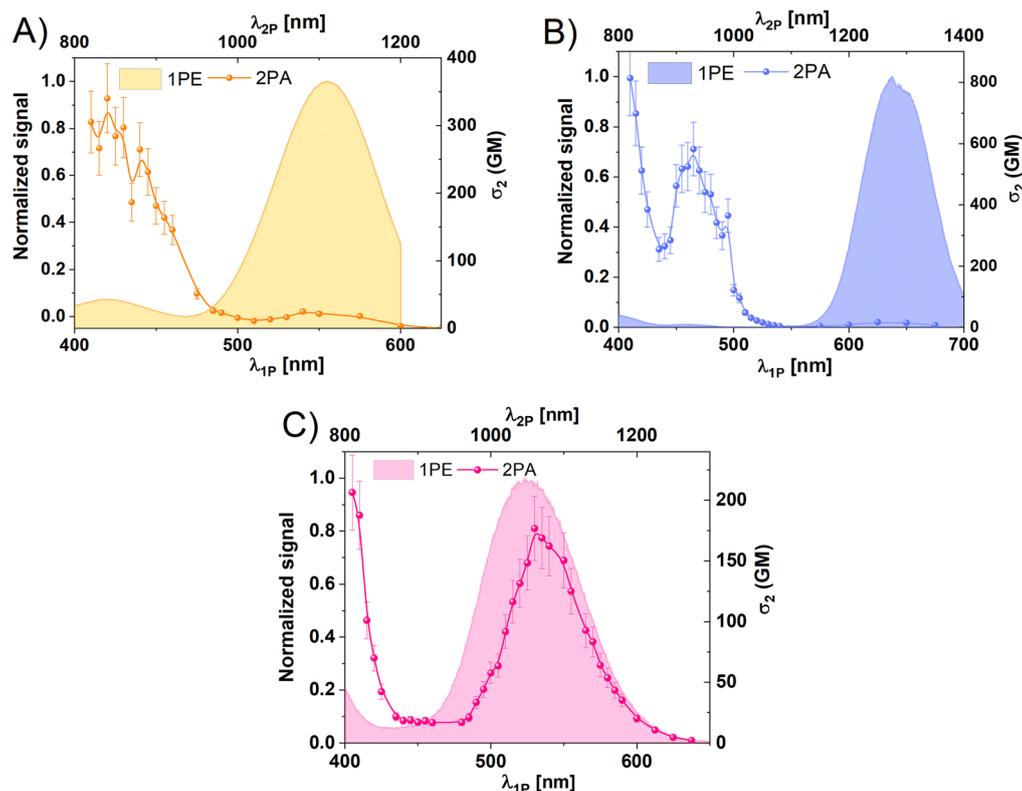

Fig. 2 Comparison between one photon excitation (1PE, filled bands) and two photon absorption (2PA, points and lines) of (A) **Ag$_{15}$-DNA**, (B) **Ag$_{21}$-DNA**, (C) **Ag$_{16}$-DNA-Cl$_2$**.
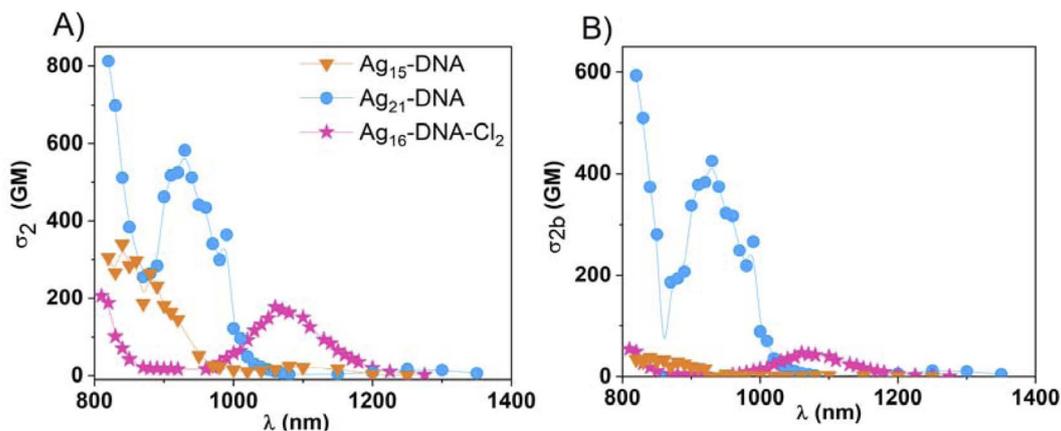
Fig. 3 Comparison of (A) two-photon absorption (2PA) cross-section (σ_2) and (B) 2PA brightness, $\sigma_{2,b}$ of Ag_{15}-DNA (orange inverted triangles), Ag_{21}-DNA (blue circles), Ag_{16}-DNA-Cl_2 (pink stars). The standard deviation of presented values is estimated to be ± 15%, not included in figures for more clarity.

electronegative atoms, chlorine influences electron density, electric transition dipole moment and increases the inter- and intra-molecular charge-transfer effects. Indeed, computational modelling[41] shows that chloridos modulate electron density and optical properties of Ag_{16}-DNA-Cl_2, stabilizing the electronic structure by reducing the electron density in the metal core and thereby leading to shifts in the nanocluster energy levels, affecting both the HOMO (highest occupied molecular orbital) and LUMO (lowest unoccupied molecular orbital) energies. Calculations also revealed that the experimentally observed absorbance peak at 525 nm consists only of a HOMO-to-LUMO molecular transition ($S_0–S_1^*$) located at the silver core of Ag_{16}-DNA-Cl_2,[41] while higher energy transitions also contain contributions from silver–base and base–silver transitions, making these transitions more complex. Ag_{16}-DNA-Cl_2 presents also complex emission, with nanosecond and microsecond components. In previous reports, excited state dynamics was probed by transient absorption (TA) spectroscopy for Ag_{16}-DNA-Cl_2, revealing that upon excitation, electrons are transferred to the Franck–Condon state and then rapidly depopulate to vibrationally hot levels of the fluorescent state within 100 fs.[51] Hot vibrational levels thermalize on a timescale of 6.2 ps. Radiative relaxation (emission) to the ground state occurs with a lifetime of 4.7 ns. In a fraction of cases, the transition to a microsecond-lived state is observed with a decay time of ca. 70 μs. TA spectra showed a positive signal between 1000–1200 nm, which blue-shifts over several ns.[51] Recently, the simulated TA spectra by Malola, et al. presented a broad peak between 1100–1400 nm related to S_1 and T_1 transitions with absorption maxima at 1244 nm and 1181 nm, respectively.[50] Because this range of wavelengths overlaps with the 2PA band of Ag_{16}-DNA-Cl_2, a possible contribution of transitions in a long-lived T_1 state in measurements at NIR wavelengths were considered. Therefore, we investigated the optical properties of Ag_{16}-DNA-Cl_2 in more detail. Standard 2PEL measurements involve the use of fs lasers with 80 MHz repetition rate, corresponding to a 12.5 ns window between consecutive pulses. Because the long-lived state in Ag_{16}-DNA-Cl_2 has 70 μs lifetime, we also performed

2PEL measurements using a laser system with a 1 kHz repetition rate (1 ms window between pulses) Fig. S6† compares 2PA spectra obtained at 1 kHz and 80 MHz laser repetition rates, which show no significant changes in σ_2 value or maximum wavelength. We do observe a slight alteration in the shape of the 2PA band at 1000–1150 nm, with higher values of σ_2 at 980–1060 nm.

Finally, 2P brightness ($\sigma_{2,b} = \phi \times \sigma_2$) of each Ag_N-DNA species was calculated and compared with commercially available probes to evaluate the potential of Ag_N-DNAs for 2PFM.[52–54] Fig. 3a and b present σ_2 and $\sigma_{2,b}$ of the Ag_N-DNA species, respectively, over a range of 810–1400 nm, which spans the NIR-I and NIR-II biological tissue transparency windows. Most notably, Ag_{21}-DNA has both high σ_2 and exceptionally high FQY compared to commonly used NIR-emitting fluorophores, resulting in the highest value of 2P brightness in the NIR-I window (ca. 582 GM at 930 nm, Fig. 3b). Ag_{16}-DNA-Cl_2

Table 2 Comparison of optical properties of Ag_N-DNAs (measured in 10 mM ammonium acetate solution, pH 7) with commercially available and water-soluble fluorescent probes with emission wavelength above 600 nm (measured in H_2O). [σ_2: 2PA cross-section, $\sigma_{2,b}$: two-photon brightness]

Probe	σ_2 [GM]	$\sigma_{2,b}$ [GM]	Emission [nm]	Excitation window
mCherry[58]	25	5.5	610	NIR-II
tdTomato[58]	108	60	581	NIR-II
Alexa Fluor (ref. 21) 647	133	44	671	NIR-II
Cy5 (ref. 21)	143	40	670	NIR-II
Cy7 (ref. 21)	200	60	779	NIR-II
Alexa Fluor (ref. 21) 680	203	73	704	NIR-II
ICG[59]	210	6.3	813	NIR-II
Cy5.5 (ref. 21)	286	60	695	NIR-II
Ag_{21}-DNA	582	425	>700	NIR-I
	17	12		NIR-II
Ag_{16}-DNA-Cl_2	211	54	>700	NIR-I
	176	45		NIR-II
Ag_{15}-DNA	340	37	650	NIR-II
	25	3		NIR-I

exhibits high $\sigma_{2,b}$ in the NIR-II window. Moreover, the combined use of **Ag₁₅-DNA** with other emitters could enable two-color, 2P imaging,[55,56] as the emission of this species is blue-shifted by 50 to 100 nm from the other three Ag$_N$-DNAs, which would enable simultaneous 2PE of two distinct probes using a single laser line.

There is a major need for water-soluble NIR-emitting probes with 2PE > 1000 nm, which currently are scarce because most available probes are insoluble in water due to the presence of highly hydrophobic units. Table 2 compares the NLO properties of the four Ag$_N$-DNA species with commercially available water-soluble dyes and fluorescent proteins used in 2PFM. σ_2 and 2P brightness values of Ag$_N$-DNAs are comparable or significantly greater than the commercial fluorescent probes. The ability of Ag$_N$-DNAs to combine water solubility with NIR-I emission, high 2P brightness, low toxicity, and functionalization *via* click-chemistry for applications such as targeted staining of certain cell lines[57] positions Ag$_N$-DNA as promising emitters to address the shortage of probes that are suitable for 2PFM.

Conclusions

We investigated the 2P properties of four atomically precise Ag$_N$-DNAs with far-red to NIR-I emission. These four species present distinct ligand compositions and valence electron counts, enabling us to probe the diversity of optical properties that may vary with nanocluster composition and structure. Ag$_N$-DNA species were measured with the same optical setup and the use of HPLC purification and ESI-MS allowed us to accurately estimate nanocluster concentration, an essential property for accurate σ_2 calculation. Thus, our results provide quantitative information to advance understanding of structure–optical properties relationship of these nanoclusters. For **Ag₁₅-DNA** and **Ag₁₆-DNA-Cl₂**, the same transitions take part in 1PA and radiative relaxation (1PA and 1PE spectra overlap). In contrast, some excited states are not involved in radiative relaxation for **Ag₂₁-DNA** and **Ag₁₉-DNA**, which results in differences in 1PA and 1PE spectra, particularly in case of **Ag₁₉-DNA**. All nanocluster species present high 2PA cross-sections. For **Ag₁₅-DNA** and **Ag₂₁-DNA**, maximum σ_2 values are obtained at the low-wavelength transitions, contrary to 1PA. In case of **Ag₁₆-DNA-Cl₂**, strong 2PA is also present at NIR-II wavelengths. For **Ag₁₉-DNA**, one-photon process contributes to excitation under fs laser illumination, and further studies on this cluster are needed to fully understand its nonlinear optical properties. At present, the relationship between nanocluster structure and two-photon properties still remains poorly understood, and additional Ag$_N$-DNA crystal structures are needed to enable theoretical studies that investigate how chemical composition and structure relate to observed 2P properties. However, our findings confirm that Ag$_N$-DNAs are a new class of promising markers for NIR imaging and 2PFM, presenting high values of two-photon brightness together with other properties beneficial for bioimaging, such as NIR emission, large Stokes shifts, and water solubility. Our findings further identify the optimal excitation wavelengths to achieve a strong 2P fluorescence signal from these emitters. A deeper understanding of their photophysics and NLO

properties could enable rational design of these unique emitters for advanced two-photon deep tissue bioimaging applications.

Methods

Synthesis and purification of Ag$_N$-DNAs

An aqueous solution of single stranded DNA oligomer and AgNO₃ in 10 mM ammonium acetate (pH 7) was prepared and incubated at room temperature for 15 minutes, followed by reduction by a freshly prepared aqueous solution of sodium borohydride (more details in ESI and Table S1†). The solution was stored in the dark at 4 °C for several days to allow the fluorescent Ag$_N$-DNA to form. Each Ag$_N$-DNA was then purified by high-performance liquid chromatography (HPLC) to obtain atomically precise Ag$_N$-DNAs. The molecular compositions of HPLC-purified Ag$_N$-DNAs were determined using negative-ion mode electrospray ionization mass spectrometry (ESI-MS). The ESI-MS methods and the mass spectra of the Ag$_N$-DNAs studied are shown in Fig. S1–S4.† The concentrations of HPLC-purified Ag$_N$-DNAs were estimated using the sample's absorption at 260 nm, the known molar extinction coefficient of the ssDNA oligomer template, and the number of DNA oligomers per nanocluster (Table 1). Detailed synthesis procedures (including concentrations of DNA oligomer and AgNO₃, and storage conditions), HPLC chromatograms, and mass spectra of Ag$_N$-DNAs are reported in ref. 5.

One-photon measurements

All measurements were carried out in 10 mM ammonium acetate solution (pH 7). Absorption spectra were recorded using a Jasco V-670 spectrophotometer. Excitation and fluorescence spectra using an FS5 Spectrofluorometer (Edinburgh Instruments) equipped with a Xenon lamp.

FQY measurements

First, the FQY of the LDS-698 in CHCl₃ was determined using an integrating sphere (FS5 Spectrofluorometer) and by the comparative method. The standard in the comparative method was DCM (4-(dicyanomethylene)-2-methyl-6-(4-dimethylami-nostyryl)-4H-pyran) in EtOH with FQY = 43.5%.[60] Finally, the FQY (ϕ) was determined using the following formula:

$$\phi_s = \phi_r \frac{f_r(\lambda_{ex})}{f_s(\lambda_{ex})} \frac{\int_{\lambda_{em}} F_s(\lambda_{em})}{\int_{\lambda_{em}} F_r(\lambda_{em})} \frac{n_s^2}{n_r^2}$$

$$f_s(\lambda_{ex}) = 1 - 10^{A_x(\lambda_{ex})}$$

where, s and r stand for the sample and reference, respectively, ϕ is the quantum yield, and n is the refractive index of the solvent, $\int_{\lambda_{em}} F(\lambda_{em})$ corresponds to the fluorescence integral of the sample or reference, and $f_i(\lambda_{ex})$ refers to the corresponding absorption factor at the excitation wavelength. The results

obtained using the comparative method and the integrating sphere were almost identical, within the standard deviation margin for the integrating sphere (2%). FQY of LDS-698 in CHCl$_3$ was 14% for the absolute method and 15.5% for the comparative method. Hence, LDS-698 was used as a standard to determine the quantum yield for **Ag$_{15}$-DNA** and **Ag$_{19}$-DNA**. For **Ag$_{21}$-DNA** and **Ag$_{16}$-DNA-Cl$_2$**, FQY values were taken from previous reports.[15,16]

NLO measurements

Two-photon excited photoluminescence (2PEL) was measured using a custom-built multiphoton setup. The excitation source was femtosecond mode-locked Ti:Sapphire laser (~100 fs, 80 MHz, Chameleon, Coherent Inc. with a wavelength range 680 to 1080 nm), combined with an optical parametric oscillator Chameleon OPO (Coherent Inc., applied in 1100–1600 nm range). The signal was collected, and emission spectra were measured with a spectrograph – Shamrock 303i (Andor) with an iDUS camera (Andor). Depending on excitation wavelength ranges, optical filters were also used: FELH0950 – Ø 25.0 mm Longpass Filter (Thorlabs), FELH0800 – Ø 25.0 mm Longpass Filter (Thorlabs). The power of the laser irradiating the sample was measured and calibrated for each wavelength. Laser power was kept at ~10 mW for most measured wavelengths, to ensure quality signal of detectors and no photobleaching. Samples were irradiated only at the time of signal collection to avoid photobleaching. The sample and reference dye were always measured at the same excitation power. 2PA cross-sections were calculated with the following equation.[45,61]

$$\sigma_{2,s} = \frac{F_{2,s} C_r \phi_r n_r^2}{F_{2,r} C_s \phi_s n_s^2} \sigma_{2,r}$$

where, r and s denote reference and sample, respectively. ϕ_r and ϕ_s is the fluorescence quantum yield. $F_{2,s}$ and $F_{2,r}$ is the integrated two-photon fluorescence intensity at a particular excitation wavelength, n is the refractive index of the solvent. C_s and C_r is the concentration of the sample and reference, respectively. Styryl 9M and LDS-698 in CHCl$_3$ were used as a reference. FQY of Styryl was taken from literature.[27] FQY of LDS-698 in CHCl$_3$ was measured for this work and is described in the FQY measurements section. 2PA cross-sections of Styryl 9M and LDS-698 were obtained from previously reported literature.[45,61] Laser system employed in additional measurements of **Ag$_{16}$-DNA-Cl$_2$** was a Coherent Ti: Sapphire Astrella regenerative amplifier combined with an OPA TOPAS Prime (Coherent) optical parametric amplifier providing tunable ~60 fs pulses at 1 kHz.

Two-photon brightness ($\sigma_{2,b}$) was calculated using the equation:

$$\sigma_{2,b} = \sigma_2 \times \phi$$

Power dependence of luminescence intensity

To confirm the two-photon nature of the observed fluorescence excited by laser pulses, we measured fluorescence intensity *vs.* incident laser excitation power and determined the power

exponent, *n*. 2PEL was collected by photon-counting avalanche photodiode (IDQ id100) or spectrograph – Shamrock 303i (Andor) with an iDUS camera (Andor). To avoid photobleaching, we recorded three separate spectra at each power or recorded for 30 s on an avalanche photodiode to detect any change in intensity. The power exponent was calculated using the equation:

$$n = \frac{\log(\text{PL intensity})}{\log(P)}$$

where PL intensity is a 2P excited photoluminescence intensity and P is the average incident laser power.

Data availability

The data that support the findings of this study are available within the article and ESI.†

Author contributions

A. H. conducted optical experiments and analysed the data. R. G. prepared and characterized atomically precise nanocluster solutions. S. M. C. and J. O. B. supervised the research, analyzed the data and acquired the funding. All authors took part in writing and editing the manuscript.

Conflicts of interest

There are no conflicts to declare.

Acknowledgements

References

1 J. T. Petty, J. Zheng, N. V. Hud and R. M. Dickson, DNA-Templated Ag Nanocluster Formation, *J. Am. Chem. Soc.*, 2004, **126**(16), 5207–5212.

2 Y. Chen, M. L. Phipps, J. H. Werner, S. Chakraborty and J. S. Martinez, DNA Templated Metal Nanoclusters: From Emergent Properties to Unique Applications, *Acc. Chem. Res.*, 2018, **51**(11), 2756–2763.

3 A. Gonzàlez-Rosell, C. Cerretani, P. Mastracco, T. Vosch and S. M. Copp, Structure and luminescence of DNA-templated silver clusters, *Nanoscale Adv.*, 2021, **3**(5), 1230–1260.

4 S. M. Copp, D. Schultz, S. Swasey, J. Pavlovich, M. Debord, A. Chiu, K. Olsson and E. Gwinn, Magic Numbers in DNA-Stabilized Fluorescent Silver Clusters Lead to Magic Colors, *J. Phys. Chem. Lett.*, 2014, **5**(6), 959–963.

5 R. Guha, A. Gonzàlez-Rosell, M. Rafik, N. Arevalos, B. B. Katz and S. M. Copp, Electron count and ligand composition influence the optical and chiroptical signatures of far-red and NIR-emissive DNA-stabilized silver nanoclusters, *Chem. Sci.*, 2023, **14**(41), 11340–11350.

6 A. Gonzàlez-Rosell and S. M. Copp, An Atom-Precise Understanding of DNA-Stabilized SilverNanoclusters, *Acc. Chem. Res.*, 2024, **57**, 2117–2129.

7 A. V. Pinheiro, D. Han, W. M. Shih and H. Yan, Challenges and opportunities for structural DNA nanotechnology, *Nat. Nanotechnol.*, 2011, **6**(12), 763–772.

8 S. M. Copp and A. Gonzàlez-Rosell, Large-scale investigation of the effects of nucleobase sequence on fluorescence excitation and Stokes shifts of DNA-stabilized silver clusters, *Nanoscale*, 2021, **13**, 4602–4613.

9 A. Gonzàlez-Rosell, S. Malola, R. Guha, N. R. Arevalos, M. F. Matus, M. E. Goulet, E. Haapaniemi, B. B. Katz, T. Vosch, J. Kondo, H. Häkkinen and S. M. Copp, Chloride Ligands on DNA-Stabilized Silver Nanoclusters, *J. Am. Chem. Soc.*, 2023, **145**(19), 10721–10729.

10 R. Guha and S. M. Copp, 12 Nucleic Acid-Templated Metal Nanoclusters, in *Modern Avenues in Metal-Nucleic Acid Chemistry*, ed. Müller, J. and Lippert, B., CRC Press, 2023, pp. 291–342.

11 P. Mastracco and S. M. Copp, Beyond nature's base pairs: machine learning-enabled design of DNA-stabilized silver nanoclusters, *Chem. Commun.*, 2023, **59**, 10360–10375.

12 M. B. Liisberg, Z. Shakeri Kardar, S. M. Copp, C. Cerretani and T. Vosch, Single-Molecule Detection of DNA-Stabilized Silver Nanoclusters Emitting at the NIR I/II Border, *J. Phys. Chem. Lett.*, 2021, **12**(4), 1150–1154.

13 J. T. Petty, C. Fan, S. P. Story, B. Sengupta, M. Sartin, J.-C. Hsiang, J. W. Perry and R. M. Dickson, Optically Enhanced, Near-IR, Silver Cluster Emission Altered by Single Base Changes in the DNA Template, *J. Phys. Chem. B*, 2011, **115**(24), 7996–8003.

14 J. T. Petty, C. Fan, S. P. Story, B. Sengupta, A. St. John Iyer, Z. Prudowsky and R. M. Dickson, DNA Encapsulation of 10 Silver Atoms Producing a Bright, Modulatable, Near-Infrared-Emitting Cluster, *J. Phys. Chem. Lett.*, 2010, **1**(17), 2524–2529.

15 S. A. Bogh, M. R. Carro-Temboury, C. Cerretani, S. M. Swasey, S. M. Copp, E. G. Gwinn and T. Vosch, Unusually large Stokes shift for a near-infrared emitting DNA-stabilized silver nanocluster, *Methods Appl. Fluoresc.*, 2018, **6**(2), 024004.

16 V. A. Neacșu, C. Cerretani, M. B. Liisberg, S. M. Swasey, E. G. Gwinn, S. M. Copp and T. Vosch, Unusually large fluorescence quantum yield for a near-infrared emitting DNA-stabilized silver nanocluster, *Chem. Commun.*, 2020, **56**(47), 6384–6387.

17 R. Weissleder, A clearer vision for *in vivo* imaging, *Nat. Biotechnol.*, 2001, **19**(4), 316–317.

18 J. V. Frangioni, *In vivo* near-infrared fluorescence imaging, *Curr. Opin. Chem. Biol.*, 2003, **7**(5), 626–634.

19 A. M. Smith, M. C. Mancini and S. Nie, Second window for *in vivo* imaging, *Nat. Nanotechnol.*, 2009, **4**(11), 710–711.

20 S. E. Crowe and G. C. R. Ellis-Davies, Longitudinal *in vivo* two-photon fluorescence imaging, *J. Comp. Neurol.*, 2014, **522**(8), 1708–1727.

21 D. Kobat, M. E. Durst, N. Nishimura, A. W. Wong, C. B. Schaffer and C. Xu, Deep tissue multiphoton microscopy using longer wavelength excitation, *Opt. Express*, 2009, **17**(16), 13354–13364.

22 D. Kobat, N. Horton and C. Xu, *In vivo* two-photon microscopy to 1.6-mm depth in mouse cortex, *J. Biomed. Opt.*, 2011, **16**(10), 106014.

23 K. W. Dunn and P. A. Young, Principles of Multiphoton Microscopy, *Nephron Exp. Nephrol.*, 2006, **103**(2), e33–e40.

24 C. Xu, W. Zipfel, J. B. Shear, R. M. Williams and W. W. Webb, Multiphoton fluorescence excitation: new spectral windows for biological nonlinear microscopy, *Proc. Natl. Acad. Sci. U.S.A.*, 1996, **93**(20), 10763–10768.

25 W. R. Zipfel, R. M. Williams and W. W. Webb, Nonlinear magic: multiphoton microscopy in the biosciences, *Nat. Biotechnol.*, 2003, **21**(11), 1369–1377.

26 J. Olesiak-Banska, M. Waszkielewicz, P. Obstarczyk and M. Samoc, Two-photon absorption and photoluminescence of colloidal gold nanoparticles and nanoclusters, *Chem. Soc. Rev.*, 2019, **48**(15), 4087–4117.

27 A. Pniakowska, K. Kumaranchira Ramankutty, P. Obstarczyk, M. Perić Bakulić, Ž. Sanader Maršić, V. Bonačić-Koutecký, T. Bürgi and J. Olesiak-Bańska, Gold-Doping Effect on Two-Photon Absorption and Luminescence of Atomically Precise Silver Ligated Nanoclusters, *Angew. Chem., Int. Ed.*, 2022, **61**(43), e202209645.

28 V. Bonačić-Koutecký and R. Antoine, Enhanced two-photon absorption of ligated silver and gold nanoclusters: theoretical and experimental assessments, *Nanoscale*, 2019, **11**(26), 12436–12448.

29 J. Olesiak-Banska, M. Waszkielewicz, K. Matczyszyn and M. Samoc, A closer look at two-photon absorption, absorption saturation and nonlinear refraction in gold nanoclusters, *RSC Adv.*, 2016, **6**(101), 98748–98752.

30 A. S. Reyna, I. Russier-Antoine, F. Bertorelle, E. Benichou, P. Dugourd, R. Antoine, P.-F. Brevet and C. B. de Araújo, Nonlinear Refraction and Absorption of Ag29 Nanoclusters: Evidence for Two-Photon Absorption Saturation, *J. Phys. Chem. C*, 2018, **122**(32), 18682–18689.

31 S. H. Yau, N. Abeyasinghe, M. Orr, L. Upton, O. Varnavski, J. H. Werner, H.-C. Yeh, J. Sharma, A. P. Shreve, J. S. Martinez and T. Goodson Iii, Bright two-photon emission and ultra-fast relaxation dynamics in a DNA-templated nanocluster investigated by ultra-fast spectroscopy, *Nanoscale*, 2012, **4**(14), 4247–4254.

32 S. A. Patel, C. I. Richards, J.-C. Hsiang and R. M. Dickson, Water-Soluble Ag Nanoclusters Exhibit Strong Two-Photon-Induced Fluorescence, *J. Am. Chem. Soc.*, 2008, **130**(35), 11602–11603.

33 X. Wang, M. B. Liisberg, G. L. Nolt, X. Fu, C. Cerretani, L. Li, L. A. Johnson, T. Vosch and C. I. Richards, DNA-AgNC Loaded Liposomes for Measuring Cerebral Blood Flow

Using Two-Photon Fluorescence Correlation Spectroscopy, *ACS Nano*, 2023, **17**(13), 12862–12874.

34 H. J. Chun, E. S. Kim and B. R. Cho, Scope and limitation of label-free multiphoton microscopy and probe-labeled two-photon microscopy for the endomicroscopic diagnosis, *Scanning*, 2014, **36**(4), 462–464.

35 H. M. Kim and B. R. Cho, Small-Molecule Two-Photon Probes for Bioimaging Applications, *Chem. Rev.*, 2015, **115**(11), 5014–5055.

36 C. Cerretani, H. Kanazawa, T. Vosch and J. Kondo, Crystal structure of a NIR-Emitting DNA-Stabilized Ag16 Nanocluster, *Angew. Chem., Int. Ed.*, 2019, **58**(48), 17153–17157.

37 C. Cerretani, M. B. Liisberg, V. Rück, J. Kondo and T. Vosch, The effect of inosine on the spectroscopic properties and crystal structure of a NIR-emitting DNA-stabilized silver nanocluster, *Nanoscale Adv.*, 2022, **4**(15), 3212–3217.

38 C. Cerretani, G. Palm-Henriksen, M. B. Liisberg and T. Vosch, The effect of deuterium on the photophysical properties of DNA-stabilized silver nanoclusters, *Chem. Sci.*, 2021, **12**(48), 16100–16105.

39 V. Rück, C. Cerretani and T. Vosch, How Inert is Single-Stranded DNA Towards DNA-Stabilized Silver Nanoclusters? A Case Study, *ChemPhotoChem*, 2024, e202400014.

40 C. Cerretani, J. Kondo and T. Vosch, Removal of the A10 adenosine in a DNA-stabilized Ag16 nanocluster, *RSC Adv.*, 2020, **10**(40), 23854–23860.

41 S. Malola, M. F. Matus and H. Häkkinen, Theoretical Analysis of the Electronic Structure and Optical Properties of DNA-Stabilized Silver Cluster Ag16Cl2 in Aqueous Solvent, *J. Phys. Chem. C*, 2023, **127**(33), 16553–16559.

42 H. Häkkinen, Atomic and electronic structure of gold clusters: understanding flakes, cages and superatoms from simple concepts, *Chem. Soc. Rev.*, 2008, **37**(9), 1847–1859.

43 A. Gonzàlez-Rosell, R. Guha, C. Cerretani, V. Rück, M. B. Liisberg, B. B. Katz, T. Vosch and S. M. Copp, DNA Stabilizes Eight-Electron Superatom Silver Nanoclusters with Broadband Downconversion and Microsecond-Lived Luminescence, *J. Phys. Chem. Lett.*, 2022, **13**(35), 8305–8311.

44 S. M. Copp, D. Schultz, S. M. Swasey, A. Faris and E. G. Gwinn, Cluster Plasmonics: Dielectric and Shape Effects on DNA-Stabilized Silver Clusters, *Nano Lett.*, 2016, **16**(6), 3594–3599.

45 N. S. Makarov, M. Drobizhev and A. Rebane, Two-photon absorption standards in the 550–1600 nm excitation wavelength range, *Opt. Express*, 2008, **16**(6), 4029–4047.

46 C. Li, *Nonlinear Optics. Principles and Applications*. 1 edn, Springer Singapore, 2016, vol. XVII, p. 386.

47 M. Drobizhev, F. Meng, A. Rebane, Y. Stepanenko, E. Nickel and C. W. Spangler, Strong Two-Photon Absorption in New Asymmetrically Substituted Porphyrins: Interference between Charge-Transfer and Intermediate-Resonance Pathways, *J. Phys. Chem. B*, 2006, **110**(20), 9802–9814.

48 M. Drobizhev, N. S. Makarov, T. Hughes and A. Rebane, Resonance Enhancement of Two-Photon Absorption in Fluorescent Proteins, *J. Phys. Chem. B*, 2007, **111**(50), 14051–14054.

49 M. Drobizhev, N. S. Makarov, S. E. Tillo, T. E. Hughes and A. Rebane, Two-photon absorption properties of fluorescent proteins, *Nat. Methods*, 2011, **8**(5), 393–399.

50 S. Malola and H. Häkkinen, On transient absorption and dual emission of the atomically precise, DNA-stabilized silver nanocluster Ag16Cl2, *Chem. Commun.*, 2024, **60**(24), 3315–3318.

51 J. Chen, A. Kumar, C. Cerretani, T. Vosch, D. Zigmantas and E. Thyrhaug, Excited-State Dynamics in a DNA-Stabilized Ag16 Cluster with Near-Infrared Emission, *J. Phys. Chem. Lett.*, 2023, **14**(17), 4078–4083.

52 S. Wang, B. Li and F. Zhang, Molecular Fluorophores for Deep-Tissue Bioimaging, *ACS Cent. Sci.*, 2020, **6**(8), 1302–1316.

53 S. Pascal, S. David, C. Andraud and O. Maury, Near-infrared dyes for two-photon absorption in the short-wavelength infrared: strategies towards optical power limiting, *Chem. Soc. Rev.*, 2021, **50**(11), 6613–6658.

54 P. A. Shaw, E. Forsyth, F. Haseeb, S. Yang, M. Bradley and M. Klausen, Two-Photon Absorption: An Open Door to the NIR-II Biological Window?, *Front. Chem.*, 2022, **10**, 921354.

55 H. Kawano, T. Kogure, Y. Abe, H. Mizuno and A. Miyawaki, Two-photon dual-color imaging using fluorescent proteins, *Nat. Methods*, 2008, **5**(5), 373–374.

56 S. E. Tillo, T. E. Hughes, N. S. Makarov, A. Rebane and M. Drobizhev, A new approach to dual-color two-photon microscopy with fluorescent proteins, *BMC Biotechnol.*, 2010, **10**(1), 6.

57 V. Rück, N. K. Mishra, K. K. Sørensen, M. B. Liisberg, A. B. Sloth, C. Cerretani, C. B. Mollerup, A. Kjaer, C. Lou, K. J. Jensen and T. Vosch, Bioconjugation of a Near-Infrared DNA-Stabilized Silver Nanocluster to Peptides and Human Insulin by Copper-Free Click Chemistry, *J. Am. Chem. Soc.*, 2023, **145**(30), 16771–16777.

58 M. Drobizhev, S. Tillo, N. S. Makarov, T. E. Hughes and A. Rebane, Absolute Two-Photon Absorption Spectra and Two-Photon Brightness of Orange and Red Fluorescent Proteins, *J. Phys. Chem. B*, 2009, **113**(4), 855–859.

59 M. Y. Berezin, C. Zhan, H. Lee, C. Joo, W. J. Akers, S. Yazdanfar and S. Achilefu, Two-Photon Optical Properties of Near-Infrared Dyes at 1.55 μm Excitation, *J. Phys. Chem. B*, 2011, **115**(39), 11530–11535.

60 K. Rurack and M. Spieles, Fluorescence Quantum Yields of a Series of Red and Near-Infrared Dyes Emitting at 600–1000 nm, *Anal. Chem.*, 2011, **83**(4), 1232–1242.

61 N. S. Makarov, J. Campo, J. M. Hales and J. W. Perry, Rapid, broadband two-photon-excited fluorescence spectroscopy and its application to red-emitting secondary reference compounds, *Opt. Mater. Express*, 2011, **1**(4), 551–563.